Electronic band structure, specific heat, and ^{195}Pt NMR studies of the filled skutterudite superconductor $ThPt_4Ge_{12}$

V. H. Tran,[1] B. Nowak,[1] A. Jezierski,[2] and D. Kaczorowski[1]
[1]*Institute of Low Temperature and Structure Research, Polish Academy of Sciences, P.O. Box 1410, 50-950 Wrocław, Poland*
[2]*Institute of Molecular Physics, Polish Academy of Sciences, 60-179 Poznań, Poland*
(Received 12 January 2009; published 9 April 2009)

Specific-heat measurements and ^{195}Pt NMR studies have been carried out for actinoid-bearing filled skutterudite superconductor $ThPt_4Ge_{12}$ with T_c=4.62 K. The lattice contribution to the total specific heat has been analyzed in terms of combination of the Einstein and Debye theories. The data show that $ThPt_4Ge_{12}$ has one optical and two acoustic vibrational modes. The numbers of such modes and the magnitudes of the vibration frequencies suggest that the two acoustic modes can be attributed to the Pt and Ge atoms forming two different cages in the cubic bcc skutterudite structure, while the optical mode can be associated with weakly bonded Th atoms occupying a center of these cages. The ^{195}Pt Knight shift and spin-lattice relaxation rates in $ThPt_4Ge_{12}$ can be understood in terms of conventional Fermi-liquid picture. Distinct anisotropy in these quantities presumably arises from $d(p)$-orbital components. The experimental data have been confronted with the electronic band structure of $ThPt_4Ge_{12}$ calculated by *ab initio* full-potential relativistic local-orbital method within the local-density approximation. Enhanced value of the mass enhancement coefficient points to considerable electron-phonon interaction and some electron-electron correlations. The Fermi surface of metallic $ThPt_4Ge_{12}$ consists of nonspherical hole and electron sheets.

DOI: 10.1103/PhysRevB.79.144510 PACS number(s): 74.25.Jb, 76.60.−k, 74.25.Bt

I. INTRODUCTION

Ternary skutterudites RT_4X_{12} (R=rare earth, T=transition metal, X=P, As, Sb) have been the subject of intensive research for many years.[1] Due to strong hybridization between 4f electrons and conduction electrons, associated with unique cage structures, some of these compounds exhibit exotic phenomena, such as intermediate valence, heavy-fermion state, Kondo semiconducting properties, non-Fermi-liquid behavior or/and superconductivity.[2–5] Most recently, superconductivity has also been discovered in a novel family of Ge-based skutterudites MPt_4Ge_{12} with M=Sr, Ba, La, Pr, and Th.[6–9] Interestingly, all these phases show similar values of the critical temperatures, which range from ~5 to ~8 K. This fact points to a minor role of the filler M element, but a dominating contribution to the superconducting properties from interactions within the cages formed by the Pt and Ge atoms.

In the skutterudites, the T and X atoms form cages rounding the guest M atoms shown in Fig. 1. There are two interesting aspects of this structure that are worthwhile to be taken into consideration. First, the bonding stabilization of the structure is owed to hybridization and electron donation between the M atoms and the T_4 and X_{12} frameworks. These factors govern the character of the conduction band and various strongly correlated electron phenomena. The second feature is the location of the filler M atom in the oversized cages. The cages are sufficiently large for loosing rigid bonds of the M atoms with the cages, and as a result these atoms exhibit incoherent vibrations, so-called rattling motion.[10]

In order to build a complete picture of the role of Pt and Ge in the physical properties of $ThPt_4Ge_{12}$, especially in the superconductivity that sets in at T_c=4.62 K, it is useful to study the behavior of these atoms within the cages they form. For this purpose, we have investigated the lattice specific heat and the nuclear magnetic resonance (NMR) on the ^{195}Pt nuclei. The experimental studies have been supplemented by band-structure calculations performed using the full-potential local-orbital (FPLO) and full-potential linearized augmented-plane wave (FP-LAPW) codes. Previously, the density of states (DOS) of $ThPt_4Ge_{12}$, calculated using *ab initio* quantum-mechanical molecular dynamics using pseudopotentials and a plane-wave basis set within the VASP package. The general finding of that study can be briefly summarized as follows: there is a strong hybridization between the Ge and Pt states, which contribute to the peak in DOS at the Fermi level E_F being equal to 9.63 states eV^{-1} f.u.$^{-1}$. According to the report, the density of states near E_F is predominantly due to germanium p- and s-like states.[9] There have been published two reports on the specific heat of $ThPt_4Ge_{12}$.[8,9] The low-temperature data indicated that the lattice specific heat follows a $C_{ph} \sim \beta T^3 + \sigma T^5$ relation,[8] where the first term is derived from the Debye model and the second term represents deviations from the T^3 approximation. This observation would imply the existence of several vibra-

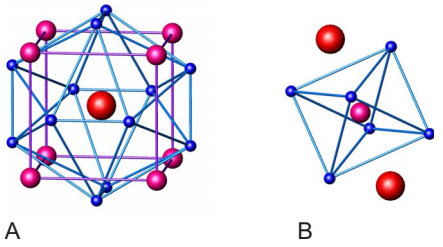

FIG. 1. (Color online) Schematic view of the filled skutterudite $ThPt_4Ge_{12}$. (a) Cages centered on the Th atoms (the biggest ball) are formed by the Pt atoms (the middle size balls) and by the Ge atoms (the smallest balls). (b) The Pt atoms are in distorted octahedral Ge coordination with distance $d_{Pt\text{-}Ge}$=2.46 Å. Two Th atoms with $d_{Pt\text{-}Th}$=3.72 Å are far away from the central Pt atom.

tional modes in $ThPt_4Ge_{12}$. Further, the high-temperature data revealed, in addition to one acoustic mode with one Debye temperature $\Theta_D=260$ K, two other optical modes with two Einstein temperatures $\Theta_{E1}=34.7$ K and $\Theta_{E2}=63.8$ K, respectively.[9] To the best of our knowledge no NMR data have been published for $ThPt_4Ge_{12}$. Most recently, ^{195}Pt NMR spectra and the temperature variations in Knight shifts and spin-lattice relaxation rates were reported for superconducting $LaPt_4Ge_{12}$ and its magnetic counterpart $CePt_4Ge_{12}$.[11] In La-based compound, the ^{195}Pt NMR spectrum shows uniaxially symmetric pattern associated with anisotropic Knight shift due to orbital contribution. The measurement also revealed some enhancement in the Korringa relation, indicating the presence of magnetic correlations. In $CePt_4Ge_{12}$, a remarkable result was the observation of an activation-type temperature dependence of the nuclear spin-lattice relaxation above 100 K and $T_1T=$const below 20 K. T_1 is the spin-lattice relaxation time. The observed behavior has been attributed to residual states at the Fermi energy existing inside the gap.

II. EXPERIMENTAL DETAILS

Polycrystalline sample of $ThPt_4Ge_{12}$ was prepared and characterized as described in Ref. 8. The specific heat was measured by the thermal-relaxation method in the temperature range between 1.8 and 300 K and in applied fields up to 2.6 T, employing a Quantum Design PPMS platform.

^{195}Pt NMR measurements were performed in the temperature range 25–300 K using a Bruker Avance DSX-300 spectrometer (operating at a field of 7.05 T) and an Oxford Instruments ITC-503 temperature controller. The spectra were obtained by the Fourier transforms of the solid echo signals produced by a sequence of two equal-width pulses $(90°)_{\pm x}-\tau-(90°)_{\pm y}$ using quadrature detection and extended phase cycling procedures.[12] The ^{195}Pt Knight shifts (K) are given with reference to Ξ ^{195}Pt=0.21400000, (IUPAC d scale).[13] Here Ξ is defined as the ratio of the isotope-specific frequency to that of ^{1}H in tetramethylsilane (TMS) in the same magnetic field.[13] More positive values of Knight shifts correspond to high-frequency, low-field, paramagnetic, deshielded values. ^{195}Pt nuclear spin-lattice relaxation times (T_1) were measured using a saturation recovery pulse sequence in which the solid echo pulse sequence has been used in position of a single monitoring 90° pulse, i.e., $(90°)_x$—variable delay $\tau-(90°)_{\pm x}-\tau-(90°)_{\pm y}-\tau$—echo. The recovery of the echo amplitude after the saturation of nuclear spins by single 90° radio-frequency (RF) pulse was found to be of single exponential form, and T_1 was determined by fitting the data to the three-parameters recovery function $M(t)=M(\infty)[1-C\exp(-t/T_1)]$. The quantities T_1, $M(\infty)$ and $C(\cong 1)$ were treated as adjustable parameters.

The electronic properties of $ThPt_4Ge_{12}$ were calculated by *ab initio* full-potential relativistic local-orbital (FPLO) method within the local-density approximation (LDA).[14–16] The exchange correlation potential was used in the form of Pardew and Wang.[17] The self-consistent potentials were carried out on a k mesh of 396 k points in each direction of the Brillouin zone. In these calculations, the valence states were assumed for 7s, 7p, 6d orbitals of Th, 6s, 6p and 5d orbitals for Pt, and 4s, 4p and 3d orbitals for Ge. It should be noted that local orbitals of Th (6s,6p), Pt (5s,5p,4f) and Ge (3s,3p) were treated as semicore states. The calculations were performed fully relativistically including the relativistic effect of spin-orbit coupling. The input parameters were the experimental room-temperature value of the lattice parameter $a=8.5924$ Å (Ref. 8) and the atomic positions 2(a) for Th, 8(c) for Pt and 24(g) for Ge with $y_{Ge}=0.1515$, $z_{Ge}=0.3556$ (Ref. 9). In addition to the FPLO analysis, the density of states in $ThPt_4Ge_{12}$ were calculated by full-potential linearized augmented-plane-wave (FP-LAPW) method within the exact-exchange density-functional theory (DFT) using the EXCITING code.[18] In these latter calculations all core-valence interactions were taken into account.

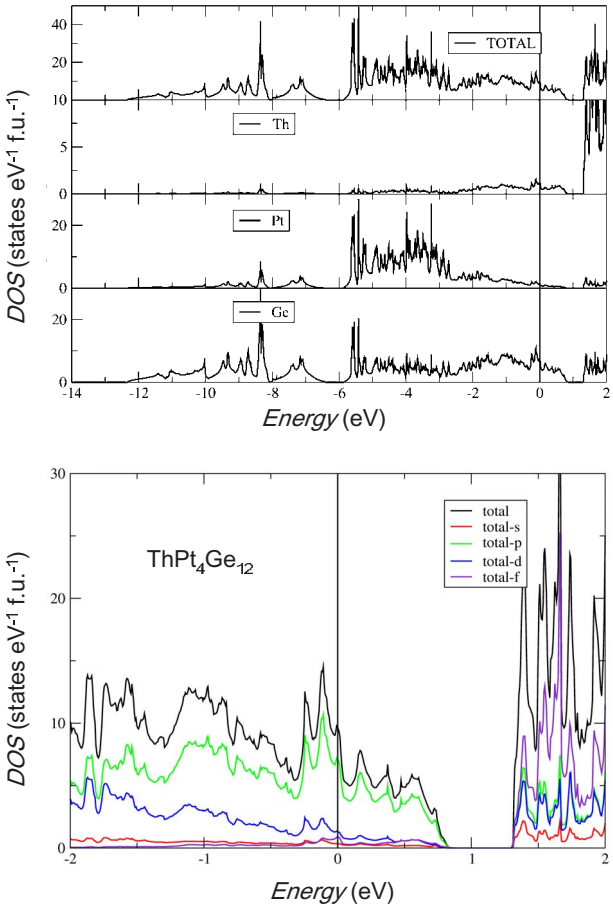

FIG. 2. (Color online) Calculated total and partial densities of states in $ThPt_4Ge_{12}$ that arise from the constituting atoms (upper panel) and from the s, p, d, and f states (lower panel).

III. RESULTS AND DISCUSSION

A. Electronic structure

The two methods applied to calculate the electronic structure $ThPt_4Ge_{12}$, i.e., FPLO and FP-LAPW, yielded very similar results, and therefore in the following only the data obtained by the FPLO code are discussed. The calculated density of states in $ThPt_4Ge_{12}$ is shown in Fig. 2. The bands

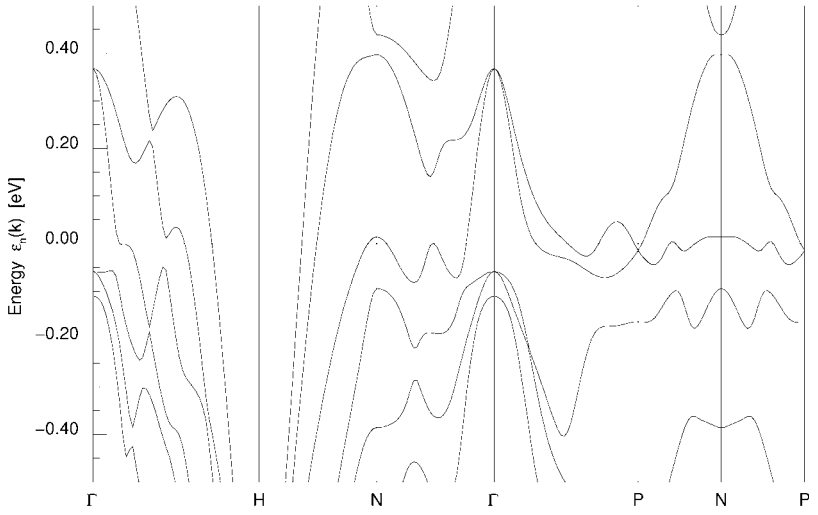

FIG. 3. Calculated energy band structure of $ThPt_4Ge_{12}$ near the Fermi level along high-symmetry lines.

up to −8 eV mainly originate from the Ge-*s* band. Between −8 eV and −6 eV the contributions of both Pt and Ge atoms are apparent. Here, the Pt-5*d* components are strongly hybridized with the Ge-3*p* and Ge-3*s* components. The contribution of the Pt-5*d* states becomes dominating in the hybridized band between −6 and −2.5 eV. The Ge-4*p* states are rather dispersive, extending from −5.5 eV to about 1 eV, and make the dominant contribution to the total density of states at the Fermi level. An interesting feature of the conduction bands of $ThPt_4Ge_{12}$ is a very sharp peak structure in DOS just below E_F. The peak arises due to hybridization between the *d* orbitals of Pt and Ge as well as the *d* and *f* orbitals of Th with the *p* orbitals of Ge and Pt. The contributions of the particular atoms to the total DOS at E_F are as follows:

(i) Th atom: 1.22 states eV^{-1} $f.u.^{-1}$ with the partial densities: 6*d*: 0.33, 5*f*: 0.85, 7*s*: 0.02, 7*p*: 0.02.

(ii) Pt atom: 1.27 states eV^{-1} $f.u.^{-1}$ with the partial densities: 6*s*: 0.11, 6*p*: 0.43, 5*d*: 0.73.

(iii) Ge atom: 7.26 states eV^{-1} $f.u.^{-1}$ with the partial densities: 4*s*: 0.25, 4*p*: 6.75, 4*d*: 0.26.

It should be noted that the Th 6*d* and 5*f* components are noticeably large near E_F (see the lower panel in Fig. 2). In particular, the contribution of the 5*f* orbital to total DOS reaches as much as 8.7% compared to 13.5% coming from the total *d* orbitals and 73.8% arising from the total *p* orbitals. In contrast, the contribution of the *s* orbitals is negligible. The obtained data suggest that the *f*-*pd* mixing interaction plays an important role in $ThPt_4Ge_{12}$, especially in the electronic conduction of this compound. One may add that the presence of the Th *f* orbital at the Fermi level was previously observed in Korringa–Kohn–Rostoker band-structure calculations for ThB_4Co.[19]

The overall characteristics of the density of states presented in Fig. 2 are similar to those reported previously.[9] However, there is an essential difference in the peak structure in DOS just below E_F. The present calculations revealed two sharp DOS features at the binding energies 0.25 and 0.1 eV, respectively, compared to the one peak structure in the previously published data. This implies that DOS near the Fermi energy is very sensitive to either the calculation method employed or to the values of the crystallographic input parameters used. The density of states at the Fermi level is estimated to be $N(E_F)=9.75$ (states eV^{-1} $f.u.^{-1}$), which corresponds to the theoretical Sommerfeld coefficient $\gamma_{\text{theo}} = \pi^2 k_B^2 N_A N(E_F)/3$ of 23 mJ mol^{-1} K^{-2}. The total electron-mass enhancement $\lambda = \frac{\gamma_{\text{exp}}}{\gamma_{\text{theo}}} - 1$ is estimated to be 0.74, which is somewhat larger than the previously reported electron-phonon enhancement factor of 0.62–0.66.[8,9] This important finding points to a considerable electron-phonon interaction and some electron-electron correlations in the compound studied.

Figure 3 displays the band structure of $ThPt_4Ge_{12}$ along various high symmetry directions in the Brillouin zone. The data reveal three bands crossing the Fermi level along the N-H direction. These bands yield a considerable density of states in the valence and conduction bands around the Fermi energy, hence reflecting a metallic nature the compound, in agreement with the experiments.[8,9]

The calculated Fermi surface of $ThPt_4Ge_{12}$ is shown in Fig. 4. There are three kinds of the Fermi surfaces, denoted in the figure as band A, B and C. The band A constructs large hole sheet centered at the Γ point, which exhibits a complex network consisting of big pockets. Rather unexpectedly for the cubic crystal structure, the Fermi surface of $ThPt_4Ge_{12}$ has no fourfold symmetry. Instead, it has sixfold symmetry along the $\Gamma - P$ axis, shown by the cross section. The band B forms four structure sheets, for which twofold symmetry is visible along the $\Gamma - P$ or $\Gamma - H$ axes. In turn, the Fermi surfaces from the band C have six sheets with two disklike and four cushionlike shapes. Such asymmetrical Fermi surfaces of bands A, B, and C are probably related to a strong hybridization of the Ge-5*p* states with the Pt-4*d* states and in a weaker strength with the Th 5*f* states. The revealed asymmetricity of the Fermi surfaces in an intriguing feature of $ThPt_4Ge_{12}$ that deserves further investigations being focused on the expected anisotropic physical properties of this compound.

B. Specific heat

The specific-heat data of $ThPt_4Ge_{12}$ are presented in Fig. 5. In the normal state, the compound is a weak diamagnet,[8]

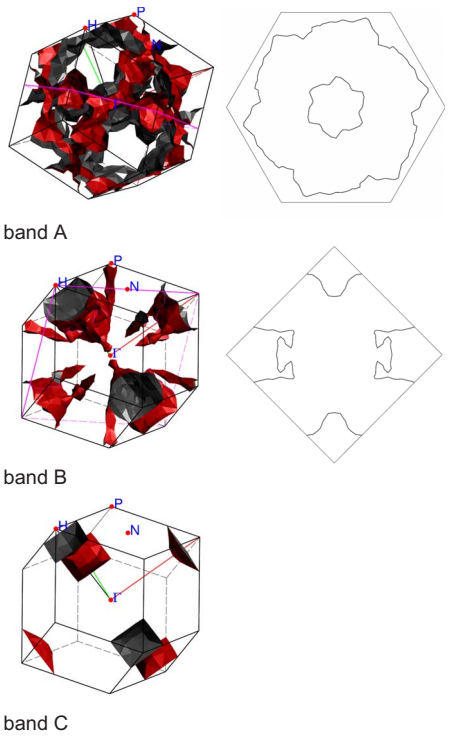

FIG. 4. (Color online) Calculated Fermi surfaces of $ThPt_4Ge_{12}$ and their cross sections. The Γ point is placed at the center of the boxes.

thus C_p above T_c is assumed to be a sum of two terms: electronic specific heat $C_{\rm el}$ and phonon specific heat $C_{\rm ph}$. The specific heat $C_{\rm el}$ can be estimated from the low-temperature data taken in a magnetic field of 0.5 T that totally suppresses the superconductivity (see the inset of Fig. 5). Fitting in this region the expression $C_p=\gamma_n T+\beta T^3+\sigma T^5$ (cf. Ref. 8) yielded $\gamma_n=40(2)$ mJ mol^{-1} K^{-2}, and the parameters $\beta=3.25(2)$ mJ mol^{-1} K^{-4} and $\sigma=0.03(1)$ mJ mol^{-1} K^{-6}. Then, by subtracting $C_{\rm el}=\gamma_n T$ from the measured C_p in the entire temperature range the phonon specific heat $C_{\rm ph}$ can be determined, as shown in Fig. 6 as the ratio $C_{\rm ph}/T3$ vs T.

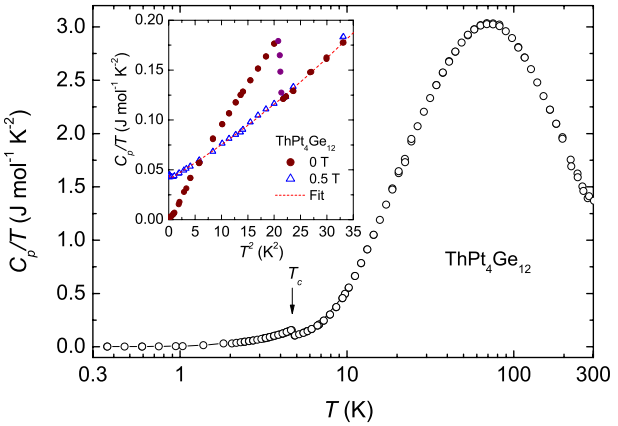

FIG. 5. (Color online) Temperature dependence of the total specific heat of $ThPt_4Ge_{12}$ divided by temperature. The inset shows the specific-heat data collected at 0 and 0.5 T as a ratio C_p/T vs $T2$. The dashed line is the low-temperature fit described in the text.

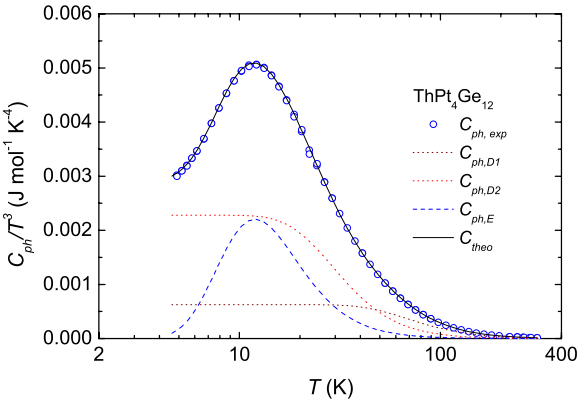

FIG. 6. (Color online) Temperature dependence of the phonon specific heat of $ThPt_4Ge_{12}$ divided by $T3$. The solid line is the fit discussed in the text. The dotted, dash-dotted, and dashed lines represent the contributions of the two acoustic and one optical modes, respectively.

In general, the lattice specific heat is due to acoustic and/or optical phonons. For a compound having n atoms per unit cell, one expects three acoustic and $3n-3$ optical modes. The acoustic modes are represented as Debye oscillators, which contribute to the total specific heat as $C_{{\rm ph},D}(T)=9Rn_D(T/\Theta_D)3\int_0^{\Theta_D/T}\frac{x^4\exp(x)}{[\exp(x)-1]^2}dx$, while the optical modes are given by the formula $C_{{\rm ph},E}(T)=3Rn_E\frac{(\Theta_E/T)^2\exp(\Theta_E/T)}{[\exp(\Theta_E/T)-1]^2}dx$, where R is the gas constant, Θ_D, Θ_E, n_D, and n_E are the Debye temperature, the Einstein temperature, the number of Debye oscillators and the number of Einstein oscillators, respectively.[20] In filled skutterudites RT_4X_{12}, the low-energy optical modes are associated with the incoherent vibrations of the R ions in the T_4X_{12} cages.[10] For $ThPt_4Ge_{12}$, the presence of such optical phonons is evidenced by a maximum around 12 K in the plot C_p/T^3 vs T (see Fig. 6).

In Ref. 9, it was argued that the phonon specific heat of $ThPt_4Ge_{12}$ can be expressed by considering one Debye and two Einstein oscillators with the characteristic temperatures $\Theta_D=260$ K, $\Theta_{E1}=34.7$ K, and $\Theta_{E2}=63.8$ K. However, it appeared not possible to describe the specific heat data obtained in the present work around the $C_{\rm ph}/T^3$ maximum, and even much worse agreement was found for temperatures between 20 and 100 K. Instead, it turned out that very good fit can be derived assuming one optical mode with $\Theta_E=59(1)$ K and $n_E=0.85(0.2)$, and two acoustic modes with $\Theta_{D1}=340(5)$ K, $n_{D1}=12.65(0.5)$ and $\Theta_{D2}=144(5)$ K, $n_{D2}=3.5(0.5)$. The description of the lattice specific heat in terms of a combination of acoustic and optical vibrational modes can be naturally associated with the specific cage crystal structure of $ThPt_4Ge_{12}$. In this compound, the Th atoms have much larger mass than the other atoms in the lattice and therefore they are expected to have a significantly lower oscillation frequency. Thus, the motion with $\Theta_E=59(1)$ K can reasonably be attributed to the Th atoms. In turn, the Pt and Ge atoms with different atomic distances to the central Th atoms ($d_{\text{Th-Ge}}=3.31$ Å and $d_{\text{Th-Pt}}=3.72$ Å) are confined to two different cages (see Fig. 1), and therefore they may have different frequencies of the oscillations. The lighter Ge atoms can be associated to the higher frequency $\Theta_{D1}=340(5)$ K,

whereas the heaver Pt atoms can be characterized by the lower frequency $\Theta_{D2}=144(5)$ K. It is worth emphasizing that such a distribution of the modes is supported by the calculated numbers of the Einstein and Debye oscillators. One may also note that the Debye temperature of 217 K, estimated in Ref. 8 from the low-temperature specific heat data, approximately corresponds to the average value of Θ_{D1} and Θ_{D2} being about 240 K. Nonetheless, in order to verify the present or hitherto proposed models of the optical and acoustic phonon modes in $ThPt_4Ge_{12}$, inelastic neutron or Raman scattering experiments are required.

C. ^{195}Pt NMR

In $ThPt_4Ge_{12}$ all the Pt atoms are crystallographically equivalent and are located at the center of distorted octahedra formed by the Ge atoms. More specifically, their point group symmetry is .–3. with threefold symmetry axis being along the one of the four [111] directions. Accordingly, the NMR spectra of the ^{195}Pt nuclei in $ThPt_4Ge_{12}$ should reveal the powder-pattern line shapes characteristic for situation when a nucleus under investigation is in an environment of axial symmetry.[21] In such a case the hyperfine interaction produces an NMR Knight shift, $K(\Theta)=K_{\rm iso}+K_{\rm ax}(3\cos^2\Theta-1)$, where $K_{\rm iso}$ and $K_{\rm ax}$ are the isotropic and axial components of the Knight shift, respectively, and Θ is the angle between the local symmetry axis and the applied magnetic field B_0. The principal components of the shift tensor are defined as

$$K_{\rm ax}=1/3(\nu_{\parallel}-\nu_{\perp})/\nu_0=1/3(K_{\parallel}-K_{\perp}), \quad (1)$$

$$K_{\rm iso}=1/3(\nu_{\parallel}+2\nu_{\perp}-3\nu_0)/\nu_0=1/3(K_{\parallel}+2K_{\perp}), \quad (2)$$

where ν_0 represents the frequency corresponding to zero Knight shift value. Here $K_{\parallel}$ and $K_{\perp}$ stand for the Knight shifts parallel and perpendicular to the symmetry axis, respectively. Then, the powder pattern shows a peak at $K_{\perp}=K_{\rm iso}-K_{\rm ax}$ and a shoulder at $K_{\parallel}=K_{\rm iso}+2K_{\rm ax}$.

The shape of the ^{195}Pt NMR spectra measured for $ThPt_4Ge_{12}$ appeared to be independent of temperature in the covered temperature range 25–300 K. For illustration, two typical spectra recorded at 50 and 200 K in a field of 7.05 T are shown in the inset of Fig. 7. For both temperatures the carrier frequency was held at the value corresponding to the resonance shift of the ^{195}Pt nuclei, $^{195}K_{\rm iso}$. As seen in Fig. 7, $K_{\rm iso}$ is positive and only weakly temperature dependent whereas the anisotropic component, $K_{\rm ax}$, is negative, small (0.05%) and almost temperature independent. The ^{195}Pt anisotropic Knight shift is a correct measure of the magnetic susceptibility anisotropy since $K_{\rm ax}\propto 1/3(\chi_{\parallel}-\chi_{\perp})_{\rm Pt}$, where $\chi_{\rm Pt}=1/3(\chi_{\parallel}+2\chi_{\perp})_{\rm Pt}$ represents the magnetic susceptibility of the Pt atoms sublattice in $ThPt_4Ge_{12}$.

In order to study the nuclear spin-lattice relaxation process of the ^{195}Pt nuclei in $ThPt_4Ge_{12}$, the NMR signal was sampled at different delay times t after the perturbation of nuclear spins by RF pulses. Some examples of such spectra are shown in Fig. 8. As might be expected, the relaxation rate $1/T_1$ of the ^{195}Pt nuclei exhibits an anisotropic behavior with $(T_1)_{\perp}\gg(T_1)_{\parallel}$. In fact, an NMR signal at $K_{\parallel}$ recovers much faster than that at $K_{\perp}$. The curve recorded after $t=15$ ms

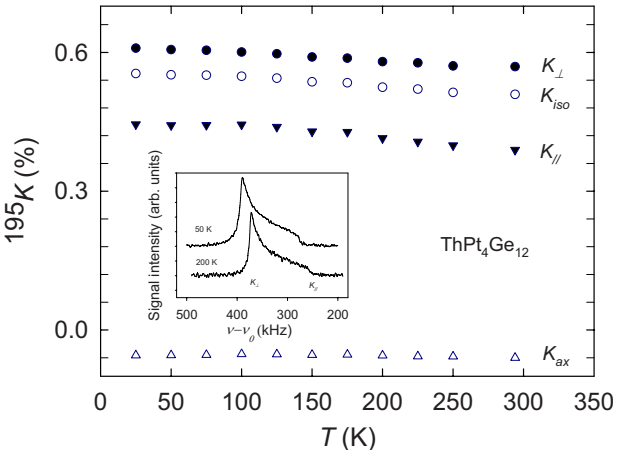

FIG. 7. (Color online) Temperature dependencies of the 195Pt Knight shift components $K_{\parallel}$, $K_{\perp}$, $K_{\rm iso}$, and $K_{\rm ax}$ in $ThPt_4Ge_{12}$. The inset presents ^{195}Pt NMR spectra recorded at 50 and 200 K in a field of 7.05 T.

(see Fig. 8) represents the NMR signal at thermal equilibrium, i.e., the signal which has completely recovered after initial saturation of the nuclear magnetization. The signal-to-noise ratio at $K_{\parallel}$ was too small to determine precisely $(T_1)_{\parallel}$, however it was sufficient to estimate $(T_1)_{\perp}$ that is longer. The obtained temperature dependence of the relaxation rate $1/(T_1)_{\perp}$ is shown in Fig. 9. Apparently $(1/T_1)_{\perp}$ varies with temperature in a linear manner, which can be understood in terms of a conventional Fermi-liquid picture.[22] This finding shows that the dominant spin-lattice relaxation process in $ThPt_4Ge_{12}$ arises from hyperfine interaction between the ^{195}Pt nuclear spins and the conduction electrons with the product $(1/T_1T)_{\perp}$ being equal to 8.5 ± 0.1 s^{-1} K^{-1}.

In elemental Pt and its alloys the main contributions to the Knight shift and the spin-lattice relaxation rate of ^{195}Pt nuclei have their origin in the following magnetic interactions:[21–32] (i) direct contact Fermi interaction of nucleus with the conduction 6s electrons, (ii) orbital and (iii) dipolar hyperfine interactions with the p and d components of conduction electron wave functions at the Fermi level, (iv) indirect contact interaction of unpaired 5d conduction elec-

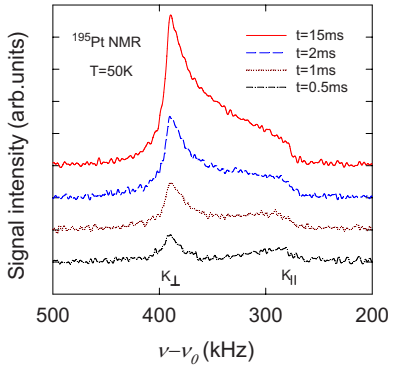

FIG. 8. (Color online) Evolution of the ^{195}Pt NMR spectra of $ThPt_4Ge_{12}$ recorded at 50 K with a few different time delays after initial saturation of the nuclear magnetization. Note an anisotropic character of the nuclear spin-lattice relaxation rate.

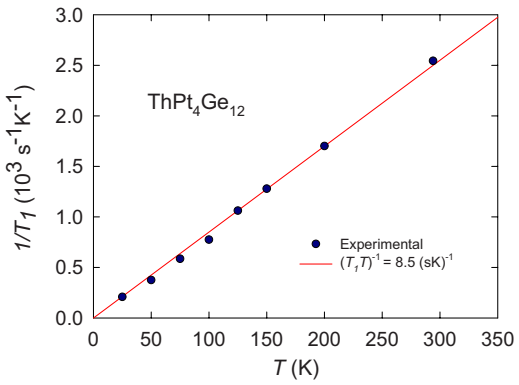

FIG. 9. (Color online) Temperature dependence of the nuclear spin-lattice relaxation rate $(1/T_1)_\perp$ for the ^{195}Pt nuclei in $ThPt_4Ge_{12}$. The solid line represents the fit with $(1/T_1T)_\perp = 8.5 \pm 0.1$ s^{-1} K^{-1}.

trons via exchange polarization of closed inner *s*-shell electrons (core polarization) and (v) conduction 6*s* electron polarization through the *s*-*d* exchange and *s*-*d* mixing interactions. The interactions (i) and (iv) are intrinsically isotropic. For local cubic symmetry, and in the absence of significant spin-orbit effects, each of these mechanisms contributes independently to the Knight shift and the spin-lattice relaxation rate:

$$K_i = (\mu_B N_A)^{-1} H_{\mathrm{hf}}(i) \chi_i, \tag{3}$$

$$\frac{1}{T_1 T}^i = 2hk_B[\gamma_n N_i(E_F) H_{\mathrm{hf}}(i)]^2 F_i, \tag{4}$$

where μ_B is the Bohr magneton, N_A is Avogadro's number, $H_{\mathrm{hf}}(i)$ are appropriate hyperfine fields (per Bohr magneton), χ_i are electronic susceptibilities, h is the Planck constant, γ_n is the nuclear gyromagnetic ratio, $N_i(E_F)$ are the partial *s*-, *p*- and *d*-bare electron state densities at the Fermi level for one direction of the spin, F_i are inhibition factors which arise from the orbital degeneracy of the $p(d)$-wave functions at the Fermi level. It is obvious that quantitative interpretation of transition-metal hyperfine effects requires a knowledge of many interaction parameters. In the case of local cubic or tetrahedral symmetry, the inhibition factors are functions of single parameter $f(t_{2g})$ or $f(e_g)$, indicating the degree of admixture of t_{2g} and e_g character of the electron *d*-wave functions at the Fermi level. In the present case, the analysis can further be complicated by the trigonal point-group symmetry of Pt atoms which make it more difficult to estimate the $p(d)$-relaxation inhibition factors. The lower symmetry leads also to an anisotropic orbital relaxation rates, as well as to interference effects.[28,29] The filled skutterudite $ThPt_4Ge_{12}$ is characterized by rather rapid nuclear spin-lattice relaxation rate and relatively small positive Knight shift. Interestingly, the derived relaxation rate (isotropic part) is comparable to that observed in elemental platinum, while the measured Knight shift is distinctly different from that in Pt. In this context it is worth recalling that platinum metal is dominated by *d*-band DOS [the literature value of $(1/T_1T)$ is 34 s^{-1} K^{-1}], whereas the Knight shift is large and negative (~−3.5% at low temperatures) being almost entirely due to core-polarization mechanism.[21,26]

As discussed above, the calculated density of states around E_F in $ThPt_4Ge_{12}$ is mainly composed of hybridized Ge 4*p*-like and Pt 5*d*-like states, and DOS has local peak structure slightly below the Fermi level (see also Ref. 9). Moreover, the relativistic effect of spin-orbit coupling does not significantly influence the band structure. For the sake of simplicity one may assume that in spite of the hybridization the wave functions at the Pt site resemble their $d(p)$ character. The magnitude of DOS related to the Pt atoms (mainly 5*p*- and 5*d*-like) calculated at E_F for one spin direction is 0.159 states/eV atom, i.e., it is only about 1/7 of that observed in Pt metal. However, there are several reasons for believing that in $ThPt_4Ge_{12}$ the *s*-contact mechanism contributes significantly to the total hyperfine interaction of the ^{195}Pt nuclei. The calculations show that the Ge 4*p* orbitals hybridize not only with Pt 5*d* but also with 6*s* orbitals, which produce a large positive Fermi contact type hyperfine field at the Pt sites. The K_{iso} and K_{ax}, as they are defined here, can be summarized by the following expressions:

$$(K_{\mathrm{iso}} = K_{\mathrm{iso}}^{\mathrm{spin}} + K_{\mathrm{iso}}^{\mathrm{orb}}), \tag{5}$$

$$(K_{\mathrm{ax}} = K_{\mathrm{ax}}^{\mathrm{spin}} + K_{\mathrm{ax}}^{\mathrm{orb}}). \tag{6}$$

$K_{\mathrm{iso}}^{\mathrm{spin}}$ is due to direct Fermi contact interaction of the ^{195}Pt nuclei with the *s*-electron conduction band ($K_{\mathrm{iso}}^{\mathrm{Fc}}$) and contribution resulting from the indirect core-polarization process ($K_{\mathrm{iso}}^{\mathrm{cp}}$) in the case of Pt *d*-band overlapping the Fermi level, i.e.,

$$K_{\mathrm{iso}}^{\mathrm{spin}} = K_{\mathrm{iso}}^{\mathrm{Fc}} + K_{\mathrm{iso}}^{\mathrm{cp}} = (\mu_B N_A)^{-1}[H_{\mathrm{hf}}(s)^{\mathrm{Pt}}\chi_s + H_{\mathrm{hf}}(\mathrm{cp})^{\mathrm{Pt}}\chi_d], \tag{7}$$

where $H_{\mathrm{hf}}(s)$ and $H_{\mathrm{hf}}(\mathrm{cp})$ represent the *s*-Fermi contact and *d*-core-polarization hyperfine fields, respectively. The *s* and *d* parts of the local spin susceptibilities, χ_s and χ_d, are given by

$$\chi_i = 2\mu_B^2 N_i(E_F)/[1 - N(E_F)V_C], \tag{8}$$

where $i=s$ or d, $^{\mathrm{Pt}}N_s(E_F)$ and $^{\mathrm{Pt}}N_d(E_F)$ are the partial *s*-band and *d*-band densities of states at the Fermi energy, respectively, while V_C represents an effective Coulomb interaction potential, which enhances the spin susceptibilities. However, in the present case $^{\mathrm{Pt}}N(E_F)V_C \ll 1$, and thus

$$K_{\mathrm{iso}}^{\mathrm{spin}} = K_{\mathrm{iso}}^{\mathrm{Fc}} + K_{\mathrm{iso}}^{\mathrm{cp}} = 2\mu_B[H_{\mathrm{hf}}(s)^{\mathrm{Pt}}N_s(E_F) + H_{\mathrm{hf}}(\mathrm{cp})^{\mathrm{Pt}}N_d(E_F)]. \tag{9}$$

For $K_{\mathrm{iso}}^{\mathrm{orb}}$ no expression of this form exists because χ_{orb} does not depend on $N(E_F)$. Actually, $\chi_{\mathrm{orb}} \sim n_o n_u/\Delta$, where n_o and n_u are the numbers of occupied and unoccupied electron states in the band, respectively, and Δ is a bandwidth.[21] The band-structure calculations (see above) clearly indicated that Pt has a nearly filled 5*d* band, which would give rise to a very small isotropic orbital shift. Qualitatively, the experimental value of $^{195}K_{\mathrm{iso}}$ can be attributed to partial cancellation between positive *s* contact plus small *d*-orbital shifts and a negative *d*-core-polarization shift. The *p*-core-polarization mechanism is usually less effective than *d* core, and thus can be ignored in this crude estimation. Assuming for the mo-

ment that the measured $^{195}K_{iso}$ is entirely due to the Fermi contact plus core-polarization mechanisms (s-d model), and taking $H_{hf}(s)=1190$ T and $H_{hf}(cp)=-119$ T as in Pt metal,[26] one obtains $K_{iso}^{Fc}=+0.69\%$, $K_{iso}^{cp}=-0.15\%$ and $^{Pt}N_s(E_F)/^{Pt}N(E_F)\equiv\rho_s=0.31$. Any small p- or d-orbital contribution to the measured $^{195}K_{iso}$ does not essentially change the magnitude of estimated parameters K_{iso}^{Fc}, K_{iso}^{cp}, and ρ_s. On the other hand, the anisotropic Knight shift and the resulting anisotropic line shape of the ^{195}Pt NMR spectra in $ThPt_4Ge_{12}$ are determined by spin-dipolar and orbital interactions K_{ax}^{spin} and K_{ax}^{orb}, respectively.[31,32]

The former is given by $K_{ax}^{spin}=2\mu_B^2N(E_F)q$, with $q=a_p\langle r^{-3}\rangle_p+a_d\langle r^{-3}\rangle_d$, where coefficients $a_{p(d)}$ are related to the angular dependent p- and d-electron partial DOS at E_F, and $\langle r^{-3}\rangle_{p(d)}$ are the expectation values of r^{-3} for the platinum electrons in a p or d state, respectively, averaged over all occupied states in the band. Quite generally,[32] $q=\langle r^{-3}\rangle_p[(4/5)x_{1,0}-(2/5)(x_{1,1}+x_{1,-1})]+\langle r^{-3}\rangle_d[(4/7)x_{2,0}+(2/7)(x_{2,1}+x_{2,-1})-(4/7)(x_{2,2}+x_{2,-2})]$, where $x_{l,m}=N_{l,m}(E_F)[\Sigma_{l',m'}N_{l',m'}(E_F)]^{-1}$. The point-group symmetry at Pt sites in $ThPt_4Ge_{12}$ is .-3. and crystal field splits the Pt d states into singlet $A_g[z^2(2,0)]$ and two doublets: $E_{1g}[x^2-y^2(2,2),xy(2,-2)]$ and $E_{2g}[xz(2,1),yz(2,-1)]$. Thus, if the d-electron spin dipolar mechanism dominates the Knight shift anisotropy, the negative value of K_{ax}^{spin} corresponds to $(x_{2,2}+x_{2,-2})>x_{2,0}+(1/2)(x_{2,1}+x_{2,-1})$. This indicates that the excess spin density at the Pt site resides on the E_{1g} band. The contribution K_{ax}^{orb} arises from the interaction of the nuclear magnetic moment and the electronic current that is induced by the external magnetic field. It reflects an anisotropy of the Van Vleck-type orbital magnetic susceptibility:

$$K_{ax}^{orb}=1/3(\mu_BN_A)^{-1}H_{hf}(orb)(\chi_{\parallel}-\chi_{\perp})_{orb}=2/3(N_A)^{-1}\langle r^{-3}\rangle_d(\chi_{\parallel}-\chi_{\perp})_{orb}. \quad (10)$$

It is assumed here that the contribution K_{ax}^{orb} arises exclusively from d electrons. Because of the large magnitude of d-orbital hyperfine field (in Pt metal $H_{hf}(orb)=110$ T; Ref. 26), only very small anisotropy of the Van Vleck susceptibility, $|(\chi_{\parallel}-\chi_{\perp})_{orb}|=7.6\times10^{-8}$ emu/mol Pt is sufficient to explain the anisotropic line shape of the ^{195}Pt NMR spectra in $ThPt_4Ge_{12}$. At present we are unable to establish the proportions between the K_{ax}^{spin} and K_{ax}^{orb} contributions to the total observed K_{ax}. Set of the same parameters, i.e., $H_{hf}(s)$, $H_{hf}(orb)$, $H_{hf}(orb)$ and ρ_s, matches also very well the magnitude of the spin-lattice relaxation rate $1/T_1T$ of the ^{195}Pt nuclei. The estimated value $\rho_s=0.31$ evidently exceeds that one determined in the band-structure calculations. However, 0.13 electrons are transferred from each Ge atom to Pt atom, indicating weakly ionic Pt-Ge bonds.[9] The contact hyperfine field should therefore be slightly larger than that assumed above, and consequently the actual value of ρ_s should be smaller.

IV. CONCLUSIONS

The analysis of the specific heat of the filled skutterudite $ThPt_4Ge_{12}$ indicated that its lattice contribution can be described with a model that assumes the Th ions as independent Einstein oscillators embedded in two different cages formed by the Pt and Ge atoms. The latter atoms oscillate as two independent Debye oscillators. In the normal state, the microscopic ^{195}Pt NMR properties of $ThPt_4Ge_{12}$ can be understood in terms of a conventional Fermi-liquid picture. All the NMR measurables, i.e., $^{195}K_{iso}$, $^{195}K_{ax}$ and $(T_1T)^{-1}$ are nearly temperature independent, alike the bulk magnetic susceptibility. From the Knight shift it follows that the dominant hyperfine coupling is largely isotropic ($^{195}K_{iso}/^{195}K_{ax}\cong10$). The p- and d-band derived density of states at the Fermi level dominates at the Pt atom sites. Consequently, both the anisotropic shift and the anisotropic relaxation rate are governed by the $d(p)$-orbital components. However, some small Pt s-electron admixture at the Fermi level is required to yield the isotropic ^{195}Pt NMR shifts and the relaxation rates to be comparable in their magnitudes to the experimentally observed values. The calculated density of states has a structure with two peaks located at about -0.25 and -0.1 eV below the Fermi level. This feature may be attributed mainly to the hybridized $p-d-f$ states. Comparison of the electronic specific-heat coefficients calculated from DOS at E_F and determined experimentally yielded an enhanced value of the total electron-mass enhancement of 0.74 that manifests strong electron-phonon interaction and possibly some electron-electron correlations. The calculated band structure indicates that $ThPt_4Ge_{12}$ is a good metal, however, the hole and electron Fermi surfaces are quite complex. Based on the observed asymmetricity of Fermi surface it is expected that the physical properties of $ThPt_4Ge_{12}$ may be anisotropic.

ACKNOWLEDGMENTS

The work was supported by the Ministry of Science and Higher Education through Research Grants No. N 202 082/0449, No. N202 116 32/3270, and No. N202 1349 33. Part of the study was performed within the frame of the National Network "Strongly correlated materials: preparation, fundamental research and applications."

[1] B. C. Sales, *Handbook on the Physics and Chemistry of Rare Earths*, edited by K. A. Gschneidner, Jr., J.-C. G. Bünzli, and V. K. Pecharsky (Elsevier, Amsterdam, 2003), Vol. 33, Chap. 211, pp. 1–34.

[2] E. Bauer, A. Galatanu, H. Michor, G. Hilscher, P. Rogl, P. Boulet, and H. Nöel, Eur. Phys. J. B **14**, 483 (2000).

[3] Y. Aoki, H. Sugawara, H. Harima, and H. Sato, J. Phys. Soc. Jpn. **74**, 209 (2005).

[4] M. B. Maple, Z. Henkie, R. E. Baumbach, T. A. Sales, N. P. Butch, P.-C. Ho, T. Yanagisawa, W. M. Yuhasz, R. Wawryk, T. Cichorek, and A. Pietraszko, J. Phys. Soc. Jpn. **77**, 7 (2008).

[5] H. Sato, D. Kikuchi, K. Tanaka, M. Ueda, H. Aoki, T. Ikeno, S.

Tatsuoka, K. Kuwahara, Y. Aoki, M. Koghi, H. Sugawara, K. Iwasa, and H. Harima, J. Phys. Soc. Jpn. **77**, 1 (2008).
[6] E. Bauer, A. Grytsiv, Xing-Qiu Chen, N. Melnychenko-Koblyuk, G. Hilscher, H. Kaldarar, H. Michor, E. Royanian, G. Giester, M. Rotter, R. Podloucky, and P. Rogl, Phys. Rev. Lett. **99**, 217001 (2007).
[7] R. Gumeniuk, W. Schnelle, H. Rosner, M. Nicklas, A. Leithe-Jasper, and Yu. Grin, Phys. Rev. Lett. **100**, 017002 (2008).
[8] D. Kaczorowski and V. H. Tran, Phys. Rev. B **77**, 180504(R) (2008).
[9] E. Bauer, Xing-Qiu Chen, P. Rogl, G. Hilscher, H. Michor, E. Royanian, R. Podloucky, G. Giester, O. Sologub, and A. P. Gonçalves, Phys. Rev. B **78**, 064516 (2008).
[10] V. Keppens, D. Mandrus, B. C. Sales, B. C. Chakoumakos, P. Dai, R. Coldea, M. B. Maple, D. A. Gajewski, E. J. Freeman, and S. Bennington, Nature (London) **395**, 876 (1998).
[11] M. Toda, H. Sugawara, K. Magishi, T. Saito, K. Koyama, Y. Aoki, and H. Sato, J. Phys. Soc. Jpn. **77**, 124702 (2008).
[12] A. C. Kunwar, G. L. Turner, and E. Oldfield, J. Magn. Reson. (1969-1992) **69**, 124 (1986).
[13] R. K. Harris, E. D. Becker, S. M. Cabral de Menezes, R. Goodfellow, and P. Granger, Solid State Nucl. Magn. Reson. **22**, 458 (2002); R. K. Harris, E. D. Becker, S. M. Cabral de Menezes, P. Granger, R. E. Hoffman, and K. W. Zilm, Solid State Nucl. Magn. Reson. **33**, 41 (2008).
[14] K. Koepernik and H. Eschrig, Phys. Rev. B **59**, 1743 (1999).
[15] H. Eschrig, *The Fundamentals of Density Functional Theory*, 2nd ed., (Edition am Gutenbergplatz, Leipzig, 2003).
[16] H. Eschrig, M. Richter, and I. Opahle, *Relativistic Solid State Calculations, Relativistic Electronic Structure Theory, Part 2. Applications*, Theoretical and Computational Chemistry Vol. 13, edited by P. Schwerdtfeger (Elsevier, New York, 2004), pp. 723–776.
[17] J. P. Perdew and Y. Wang, Phys. Rev. B **45**, 13244 (1992).
[18] J. K. Dewhurst, S. Sharma, and C. Ambrosch-Draxl, EXCITING Code Version 0.9.224, http://exciting.sourceforge.net
[19] D. Benea, V. Popa, and O. Isnard, J. Magn. Magn. Mater. **320**, 36 (2008).
[20] E. S. R. Gopal, *Specific Heats at Low Temperatures* (Plenum, New York, 1996).
[21] G. C. Carter, L. H. Bennett, and D. J. Kahan, *Metallic Shifts in NMR, Progress in Materials Science* (Pergamon, New York, 1977), Vol. 20.
[22] J. Korringa, Physica **16**, 601 (1950).
[23] Y. Obata, J. Phys. Soc. Jpn. **18**, 1020 (1963).
[24] Y. Yafet and V. Jaccarino, Phys. Rev. **133**, A1630 (1964).
[25] A. Narath, Phys. Rev. **162**, 320 (1967).
[26] B. N. Ganguly, Phys. Rev. B **8**, 1055 (1973).
[27] T. Asada, K. Terakura, and T. Jarlborg, J. Phys. F: Met. Phys. **11**, 1847 (1981).
[28] T. Asada and K. Terakura, J. Phys. F: Met. Phys. **12**, 1387 (1982).
[29] R. Markendorf, C. Schober, and W. John, J. Phys.: Condens. Matter **6**, 3965 (1994).
[30] B. Nowak, Solid State Nucl. Magn. Reson. **21**, 53 (2002).
[31] J. W. Ross, F. Y. Fradin, L. L. Isaacs, and D. J. Lam, Phys. Rev. **183**, 645 (1969).
[32] H. Ebert, J. Abart, and J. Voitländer, J. Phys. F: Met. Phys. **16**, 1287 (1986).